© 2017. Published by The Company of Biologists Ltd | Journal of Cell Science (2017) 130, 2468-2480 doi:10.1242/jcs.202812

RESEARCH ARTICLE

Smooth muscle function and myosin polymerization

Pasquale Chitano[1], Lu Wang[1,2], Gabrielle Y. Y. Tin[1], Mitsuo Ikebe[3], Peter D. Paré[1,2] and Chun Y. Seow[1,4,*]

ABSTRACT

Smooth muscle is able to function over a much broader length range than striated muscle. The ability to maintain contractility after a large length change is thought to be due to an adaptive process involving restructuring of the contractile apparatus to maximize overlap between the contractile filaments. The molecular mechanism for the length-adaptive behavior is largely unknown. In smooth muscle adapted to different lengths we quantified myosin monomers, basal and activation-induced myosin light chain (MLC) phosphorylation, shortening velocity, power output and active force. The muscle was able to generate a constant maximal force over a two fold length range when it was allowed to go through isometric contraction/relaxation cycles after each length change (length adaptation). In the relaxed state, myosin monomer concentration and basal MLC phosphorylation decreased linearly, while in the activated state activation-induced MLC phosphorylation and shortening velocity/power output increased linearly with muscle length. The results suggest that recruitment of myosin monomers and oligomers into the actin filament lattice (where they form force-generating filaments) occurs during muscle adaptation to longer length, with the opposite occurring during adaptation to shorter length.

KEY WORDS: Myosin phosphorylation, Length adaptation, Force–velocity properties, Biochemistry

INTRODUCTION

Smooth muscle has a large working length range (Uvelius, 1976; Ishii and Takahashi, 1982; Pratusevich et al., 1995). It is believed that this is made possible by length adaptation – a process that involves structural rearrangement of contractile and cytoskeletal proteins within the muscle cells (Pratusevich et al., 1995; Gunst et al., 1995; Gunst and Wu, 2001; Tang and Gunst, 2001; Tang et al., 2002; Kuo et al., 2003; Fabry and Fredberg, 2003; Gunst and Fredberg, 2003; Bai et al., 2004; Opazo Saez et al., 2004; Seow, 2005; Bursac et al., 2005; Silveira et al., 2005; Smolensky et al., 2005; Deng et al., 2006; Zhang and Gunst, 2006; Chen et al., 2010; Seow and Fredberg, 2011; Yamin and Morgan, 2012; Huang et al., 2014). Isometric force generation by smooth muscle is independent of muscle length after adaptation (Pratusevich et al., 1995; Wang et al., 2001), while shortening velocity, power output and the rate of ATP utilization are positively and linearly related to the adapted length (Pratusevich et al., 1995; Kuo et al., 2003). Length adaptation also leads to shifting of the length–force and force–velocity relationships (Wang et al., 2001; Herrera et al., 2005), indicating changes in the underlying structure of the contractile apparatus.

Milton et al. (2011) showed that there is a substantial pool of functional myosin monomers that can be converted into filaments in cultured smooth muscle cells, suggesting that normal function of smooth muscle involves myosin polymerization and depolymerization. It is possible that in adaptation to a longer length where more contractile units are needed, myosin monomers are recruited into the actin filament lattice where local conditions favor formation of filaments. However, in intact smooth muscle cells Horowitz et al. (1994) found that the amount of monomeric myosin was insignificant and the monomer concentration did not change between the relaxed or activated states. This led to the conclusion that myosin polymerization and depolymerization did not play a significant role in regulating the contraction/relaxation cycle in smooth muscle *in situ* (Horowitz et al., 1994). It is not clear what underlies the discrepancy between these two studies. One possibility is that different muscle preparations were used in the studies, i.e. cultured cells (Milton et al., 2011) versus tissue cells (Horowitz et al., 1994). Another possibility is the different cell types used; Horowitz et al. used avian gizzard smooth muscle, whereas mammalian airway smooth muscle was used by Milton et al. In neither study was the concentration of myosin monomers examined at different cell lengths.

One well known fact about smooth muscle activation is that phosphorylation of the 20 kDa regulatory myosin light chain (MLC) is a crucial step in initiating the ATP-dependent interaction between myosin motors and actin filaments (Frearson et al., 1976; Ikebe et al., 1977; Sobieszek, 1977). It is commonly accepted that the level of MLC phosphorylation is a good index for muscle activation (Mitchell et al., 2001). By measuring the level of MLC phosphorylation and power output at different adapted muscle lengths, it is possible to deduce the level of participation of myosin motors (power generators) in the contraction process and whether cell length is a determinant in myosin distribution across the different structural domains within a muscle cell. In the present study we examined MLC phosphorylation and estimated the quantity of myosin monomers as functions of cell length in length-adapted airway smooth muscle tissue under relaxed and activated conditions. We also examined the relationship between the muscle's power output and the level of activation-induced MLC phosphorylation. Data gathered in the present study are discussed with the help of a model that integrates biophysical and biochemical properties of the muscle at different adapted lengths, and delineates a simple molecular scheme to explain the mechanism of length adaptation related to subcellular processes of myosin movement into and out of the contractile filament lattice.

RESULTS

Stress–length relationships in adapted muscle strips

Before force–velocity properties and MLC phosphorylation were measured, each of the muscle strips was adapted at reference length (L_{ref}) to obtain maximal active force (F_{max}) (Fig. 1). The muscle

[1]Centre for Heart Lung Innovation – St Paul's Hospital, University of British Columbia, Vancouver, BC, Canada, V6Z 1Y6. [2]Respiratory Division, Department of Medicine, University of British Columbia, Vancouver, BC, Canada, V6Z 1Y6. [3]Department of Cellular and Molecular Biology, University of Texas Health Science Center, Tyler, TX 11937, USA. [4]Department of Pathology and Laboratory Medicine, University of British Columbia, Vancouver, BC, Canada, V6Z 1Y6.

*Author for correspondence (chun.seow@hli.ubc.ca)

G.Y.Y.T., 0000-0002-4019-2428; C.Y.S., 0000-0002-9653-8520

Received 21 February 2017; Accepted 1 June 2017

Journal of Cell Science

Journal of Cell Science (2017) 130, 2468-2480 doi:10.1242/jcs.202812

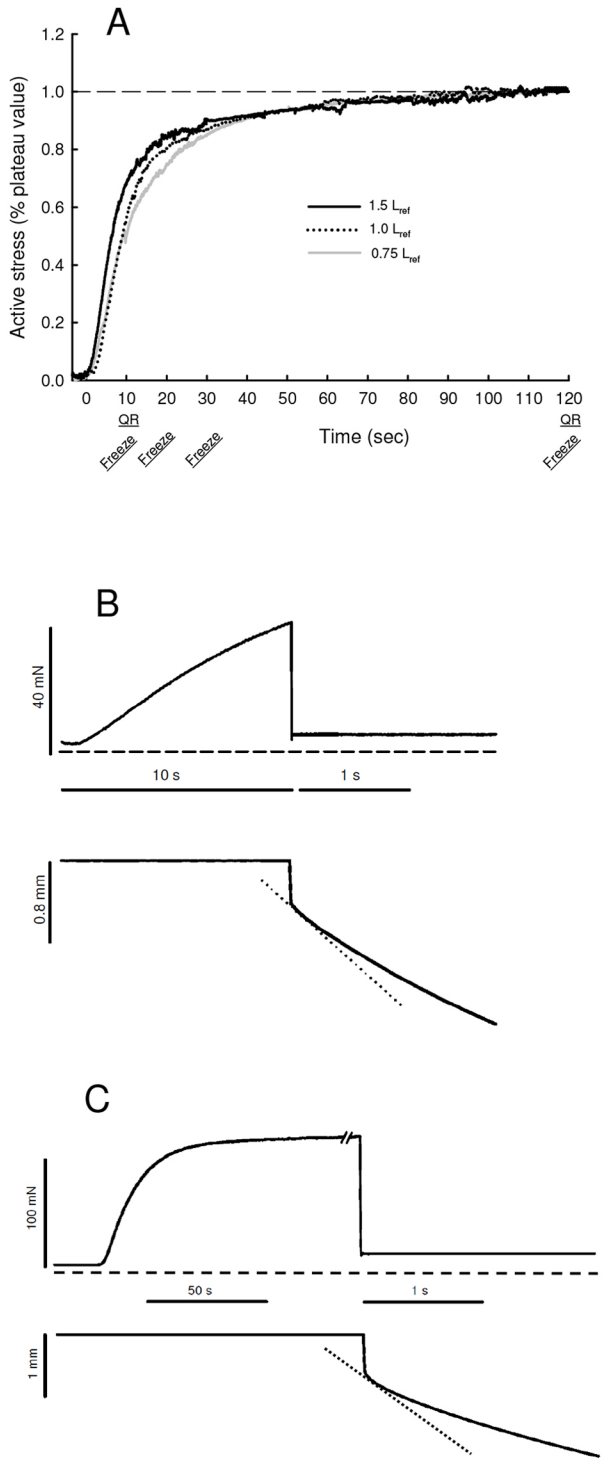

Fig. 1. Examples of force and length records. (A) Raw data showing the time course of typical isometric contractions induced by ACh at three adapted lengths (0.75, 1.0 and 1.5L_{ref}). Isotonic quick releases (QR) for measurement of force–velocity properties were carried out at two time points, 10 and 120 s, as indicated. MLC phosphorylation measurements were made at four time points indicated by the 'Freeze' labels on the graph. The average maximal stress values (and SD) are as follows (in kPa): 190.6±98.9 for 0.75L_{ref}, 191.2±51.6 for L_{ref} and 207.0 ±26.3 for 1.5L_{ref}; n=6 for each length. (B,C) Examples (raw data) of isotonic quick releases applied at 10 and 120 s, respectively, after the onset of isometric contractions induced by ACh stimulation. Upper trace in each panel: force record; dashed line indicates zero-force baseline. Lower trace in each panel: length record; the slope of the tangent (dotted line) measured at 0.1 s after the quick release was taken as the velocity of active shortening produced by the muscle.

length was then changed to either 0.75 or 1.5L_{ref} and adapted at each length. The results are shown in Fig. 2. In all groups (Fig. 2A–E) frozen for MLC phosphorylation measurement, the muscle preparations exhibited normal adaptive behavior, i.e. the values of F_{max} became independent of muscle length after length adaptation, as we have demonstrated previously (Pratusevich et al., 1995; Wang et al., 2001).

Force–velocity and force-power relationships

Fig. 3A and C show examples of force–velocity data obtained at 10 and 120 s after stimulation, respectively. The Hill hyperbolae were fitted to the data obtained at L_{ref} (Fig. 3A and C, gray symbols, dashed curves) and scaled to fit short (open symbols, dotted curves, Fig. 3A and C), and long length (black symbols, continuous curves, Fig. 3A and C). The scaling factor therefore represents changes in velocity at all loads, including zero-load velocity (V_{max}). The method of fitting by scaling the velocity values is valid only if the curvature of the force–velocity curve does not change at different adapted lengths (Pratusevich et al., 1995). The good fits obtained at 0.75 and 1.5L_{ref} indicate no change in the curvature of the force–velocity relationship at the three lengths, suggesting that there was no change in the kinetics of actomyosin interaction at the level of cross-bridge cycle (Seow, 2013). This information from curve fitting was used later in the interpretation of the force–velocity data. Fig. 3B and D show force–power relationships obtained at 10 and 120 s after stimulation at the three adapted lengths. These curves were obtained by multiplying the force and velocity values from the corresponding curves in Fig. 3A and C.

Fig. 3E and F show summarized results of maximal shortening velocity (V_{max}) and maximal power (P_{max}) obtained from force–velocity and force–power data such as those shown in Fig. 3A–D at the three adapted lengths and two different times during contraction (n=5). A significant increase in both V_{max} and P_{max} with increasing adapted length was found (P<0.001, two-way ANOVA). P_{max} was also significantly greater (P<0.001, two-way ANOVA) at 10 s after stimulation (early in contraction before the force reached plateau) compared with 120 s (force plateau). Details of the statistical analysis are given in the legend to Fig. 3.

Negative and positive staining for myosin monomers

As a negative control, primary antibody (mm19) was omitted in the staining protocol on one section obtained from an intact muscle strip fixed at L_{ref} in the relaxed state. As shown in Fig. 4A, the negative control showed negligible staining. Fig. 4B shows substantial staining for myosin monomers in intact muscle cells in the relaxed state.

Depolymerization of myosin filaments is known to occur when the filaments are exposed to high concentrations of ATP and EGTA (Cande et al., 1983). Sections of muscle after 5, 15, 30, 60 and 240 min of Triton skinning were used as a positive control and confirmation of the time course of filamentous myosin transitioning to monomeric form during skinning. As shown in Fig. 4C, contact with the skinning solution, which contained 5 mM ATP and 2 mM EGTA, caused filamentous myosin to depolymerize and high concentrations of monomeric myosin to first appear around the edges of the muscle bundle, and then spread towards the center as the skinning time increased, reflecting the diffusion process of the cell membrane-permeabilizing agent (Triton X-100), which allowed direct exposure of myosin filaments to the depolymerizing agents ATP and EGTA. At 60 min, the entire cross-section of the muscle was covered with monomeric myosin staining. This is

Journal of Cell Science (2017) 130, 2468-2480 doi:10.1242/jcs.202812

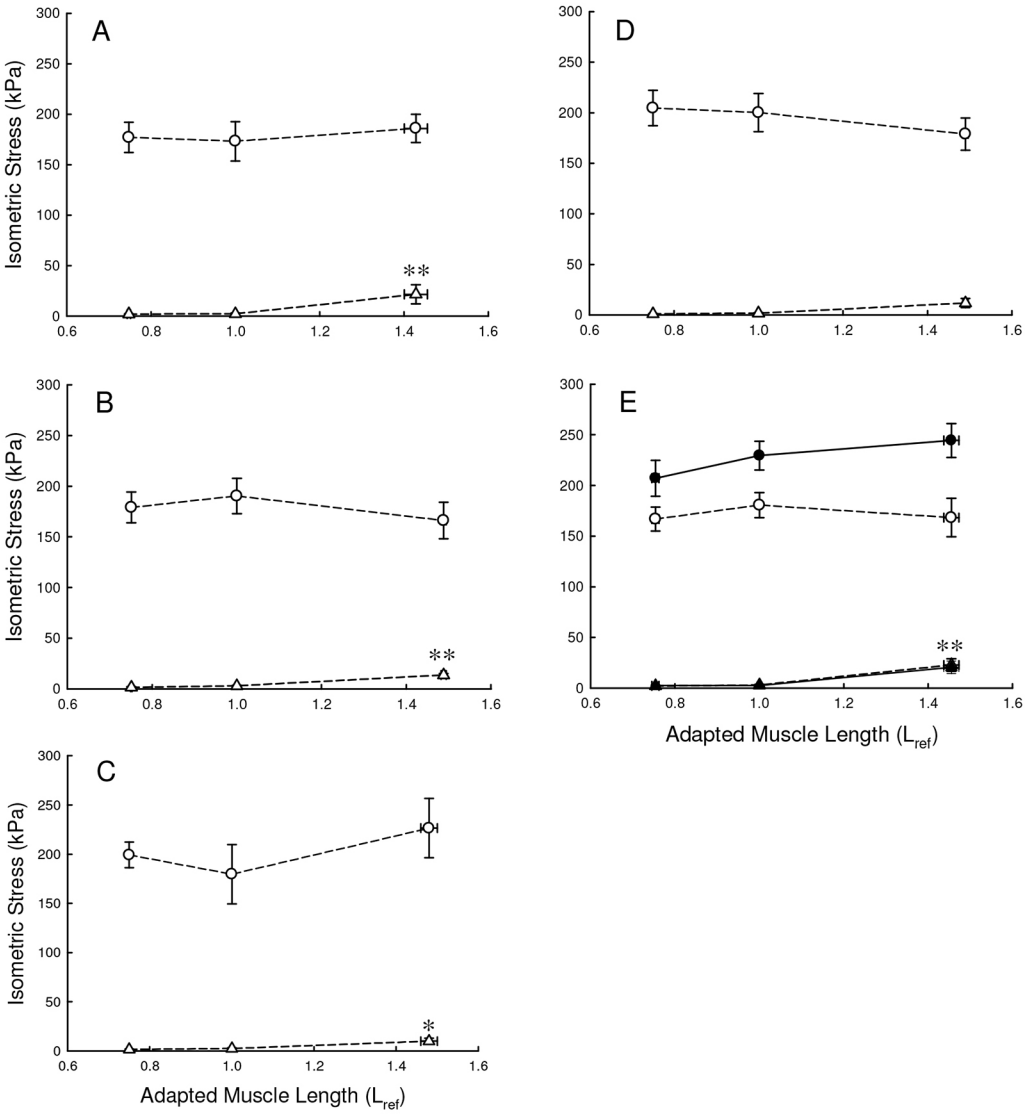

Fig. 2. Active and passive stress as functions of adapted muscle length of all muscle strips before they were frozen under different conditions for assessment of MLC-phosphorylation. Circles denote active stress; triangles denote passive stress. Open circles represent stress induced by EFS; filled circles represent stress induced by ACh; open and filled triangles represent the corresponding resting stress before activation. (A) Stress–length relationship determined before freezing in the relaxed state for determination of baseline MLC phosphorylation; n=11. (B) Stress–length relationship determined before force–velocity measurements and freezing at 10 s after ACh stimulation; n=11. (C) Stress–length relationship determined before freezing at 20 s after ACh stimulation; n=6. (D) Stress–length relationship determined before freezing at 30 s after ACh stimulation; n=6. (E) Stress–length relationship determined before force–velocity measurements and freezing at 120 s after ACh stimulation; n=16. The active stress values (in panels A–E) were all independent of the adapted lengths (one-way ANOVA, P values are between 0.263 and 0.760). For passive stress at $1.5L_{ref}$, some values are significantly higher than those at 0.75 and $1.0L_{ref}$. *P<0.05; **P<0.001; n is the number of muscle strips from different tracheas. A greater number of muscle strips was used in the 10 and 120 s groups because some of the strips used for force–velocity measurements were also frozen for the determination of MLC phosphorylation.

consistent with the electron microscope images (Fig. 5) where no filamentous myosin could be identified in the cross-sections of muscle strips fixed after 60 min of skinning. At 240 min, extensive loss of myosin monomers to the incubating solution due to diffusion can be observed (Fig. 4C). These results indicate that the monoclonal antibody, mm19, which recognizes monomeric myosin relatively specifically, can be used to estimate the concentration of monomeric myosin in the muscle cells.

Changes in staining intensity of myosin monomers in intact muscle cells adapted at different lengths

Using mm19, we estimated the monomeric myosin concentration in intact muscle cells adapted to different lengths. Fig. 6 shows mm19 staining intensity in muscle cells within the tracheal smooth muscle tissue as a function of adapted tissue length (see Materials and Methods for details on how to convert staining intensity to a percentage of maximal myosin concentration). There was a significant linear decrease (ANOVA, P=0.021, R^2=0.999) of monomeric myosin concentration with increasing adapted length. The concentration at $1.5L_{ref}$ was significantly lower than that at either L_{ref} or $0.75L_{ref}$. Details of the statistical analysis are given in the legend to Fig. 6.

MLC phosphorylation at different adapted lengths

Fig. 7A shows examples of acetylcholine (ACh)-induced MLC phosphorylation at short ($0.75L_{ref}$)-and long ($1.5L_{ref}$)-adapted muscle lengths at different time points after stimulation. The phosphorylation at all time points was significantly higher at $1.5L_{ref}$ compared with that at 0.75 and $1.0L_{ref}$ (P<0.001, two-way ANOVA) (Fig. 7B); there was also a significant decrease over time in the level of phosphorylation for the $1.5L_{ref}$ group (P<0.01, two-way ANOVA). Details of the statistical analysis are given in the legend to Fig. 7.

Fig. 7C shows MLC phosphorylation as a function of adapted muscle length (0.75, 1.0 and $1.5L_{ref}$) obtained at rest, and at 10 and 120 s after ACh stimulation. A significant (P<0.05, one-way ANOVA) linear decrease in basal phosphorylation was observed with increasing length, whereas a significant (P<0.05, one-way ANOVA) linear increase in ACh-induced phosphorylation occurred with increasing length at both time points (10 and 120 s).

When the values of V_{max}, P_{max} and ACh-induced MLC phosphorylation obtained at both 10 and 120 s after stimulation were normalized by their own reference values (obtained at L_{ref}), and plotted against the adapted muscle length, linear and positive length-dependent (P<0.001) relationships were observed (Fig. 7D).

Journal of Cell Science (2017) 130, 2468-2480 doi:10.1242/jcs.202812

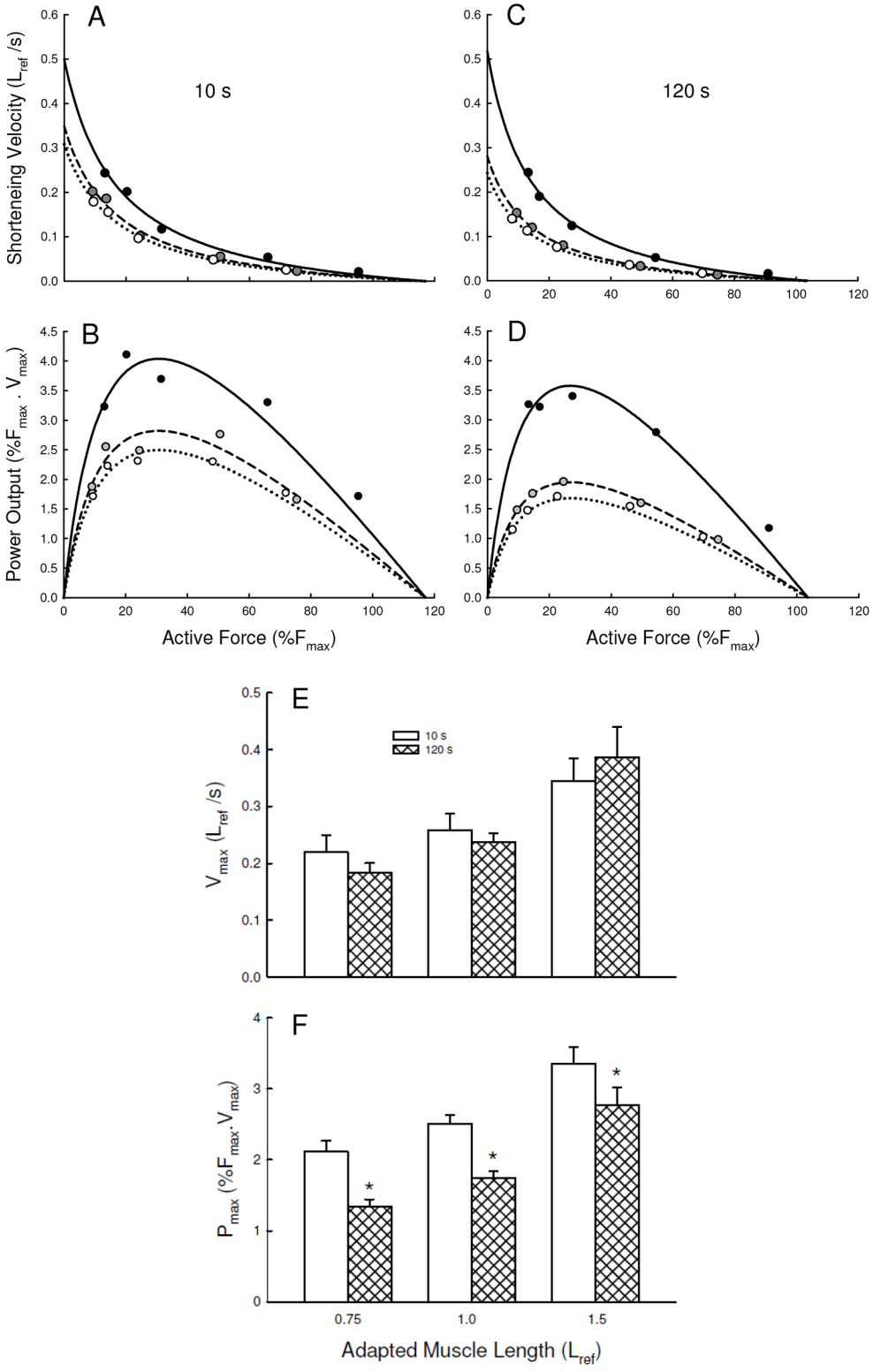

Fig. 3. Velocity and power measurements. (A) Examples of force–velocity curves obtained at L_{ref} (gray circles and dashed line), $0.75L_{ref}$ (open circles), and $1.5L_{ref}$ (filled circles) 10 s after ACh stimulation. The Hill hyperbola was used to fit the data obtained at L_{ref} (dashed line); the velocity values of the L_{ref} curve were scaled vertically down and up to fit the data obtained at $0.75L_{ref}$ (dotted curve) and $1.5L_{ref}$ (continuous curve), respectively. (B) Force–power curves derived from panel A by multiplying force and velocity values (i.e. power=force×velocity). The peak value of each curve was taken as maximal power (P_{max}) for the corresponding adapted length. (C) Examples of force–velocity curves obtained at 120 s after ACh stimulation. Symbol designation is the same as that in panel A. (D) Force–power curves derived from panel C by multiplying force and velocity values. (E) Maximal shortening velocity (V_{max}) extrapolated from force–velocity data obtained at different adapted muscle lengths and times after stimulation by ACh. In both the 10 and 120 s groups, V_{max} is significantly increased with adapted lengths (two-way ANOVA, $P<0.001$), but there is no difference between the two groups ($P=0.857$). (F) Maximal power output (P_{max}) obtained at different adapted lengths and times after stimulation by ACh. In both the 10 and 120 s groups, P_{max} is significantly increased with adapted lengths (two-way ANOVA, $P<0.001$), and there is a significant difference between the groups ($P<0.001$). There is no interaction between time after stimulation and adapted lengths ($P=0.827$). *Difference ($P<0.05$) between the values obtained at the same length but different times.

The values within each length group (measured at different times after stimulation) were not statistically different. Details of the statistical analysis are given in the legend to Fig. 7.

DISCUSSION

The results of this study show, for the first time, that a significant pool of myosin monomers co-existing with filamentous myosin is present in intact airway smooth muscle. Milton et al. (2011) provided evidence for such a pool of myosin monomers in cultured airway smooth muscle cells. In the present study we provide further evidence suggesting that interconversion of monomeric, oligomeric and filamentous myosin occurs during length adaptation. Examination of MLC phosphorylation and the mechanical properties of the muscle during length adaptation allowed us to link the myosin evanescence to cell function.

Journal of Cell Science (2017) 130, 2468-2480 doi:10.1242/jcs.202812

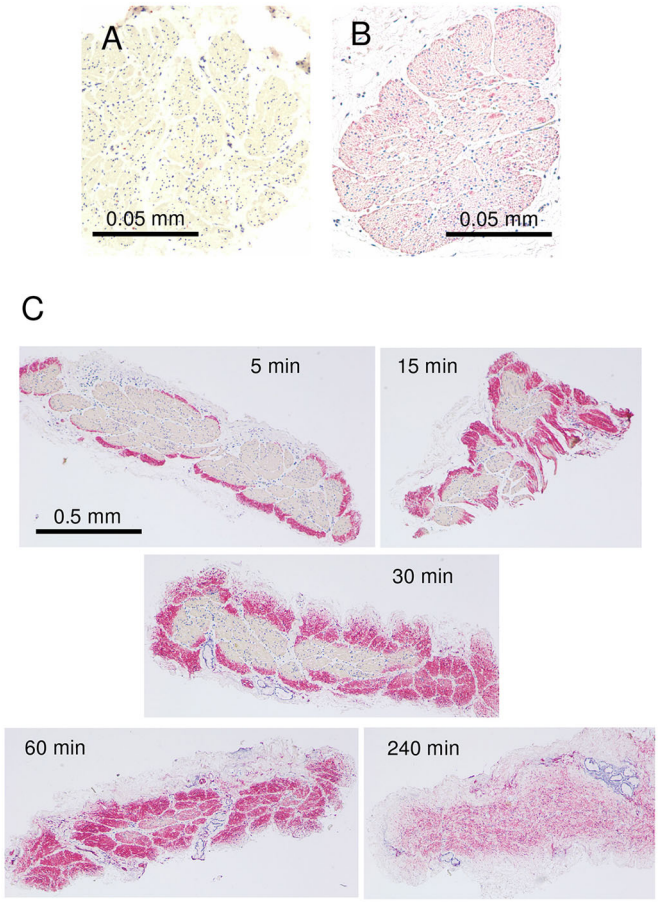

Fig. 4. Control observations for mm19 antibody staining for monomeric myosin in sheep tracheal smooth muscle. (A) Negative control staining of intact muscle cross-section without primary antibody (mm19). (B) Staining of intact muscle cross-section with mm19 antibody. (C) Staining of skinned smooth muscle bundles (cross-sections) with mm19 at different times after incubation of muscle with skinning solution.

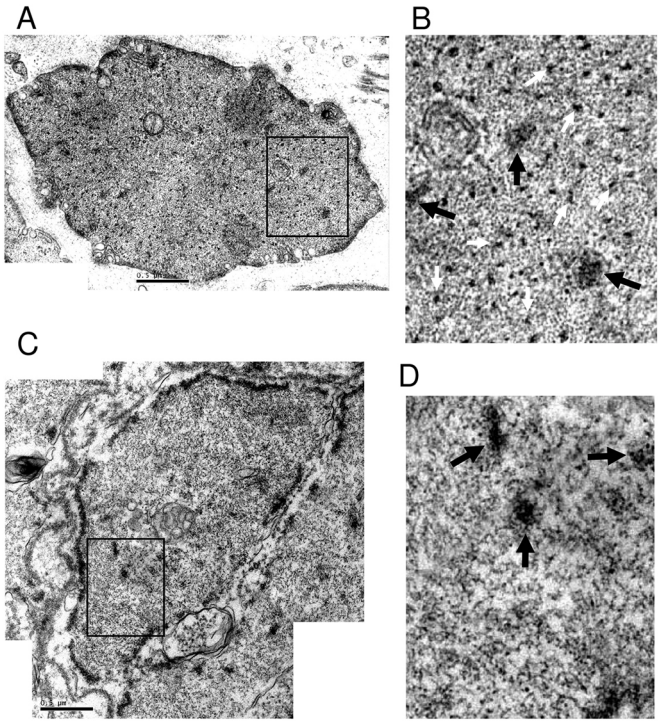

Fig. 5. Electron micrographs of cross-sections of sheep tracheal smooth muscle cells. (A) An example of intact (non-skinned) trachealis. A total of four tracheas were used in this group of study. (B) Enlarged area shown in panel A. (C) An example of skinned trachealis (fixed after 60 min of skinning). A total of four tracheas were used for this group of study. (D) Enlarged area shown in panel C. Scale bar: 0.5 µm. Black arrows point to dense bodies; white arrows point to myosin filaments. Note: no myosin filaments could be identified in panel D.

Our recent studies suggested that the resting level of MLC phosphorylation might be related to the concentration of myosin monomers (Lan et al., 2013). Review of the literature reveals that 10–20% of MLC phosphorylation is regularly observed in relaxed smooth muscle with no active tension (Gerthoffer and Murphy, 1983; Silver and Stull, 1984; Hathaway and Haeberle, 1985; Ratz et al., 1989; Ekmehag and Hellstrand, 1989; Fischer and Pfitzer, 1989; Adam et al., 1990; Abe et al., 1991; Washabau et al., 1994; Taggart et al., 1997; Mehta et al., 1998; Chitano et al., 2005). The fact that a significant portion of MLC could be phosphorylated without causing tension development may be related to a threshold of MLC phosphorylation that must be overcome during muscle activation (Warshaw et al., 1990), perhaps due to a cooperative mechanism suggested by Rembold et al. (2004). However, this mechanism does not explain why basal phosphorylation exists in resting smooth muscle in the first place. In the studies of Lan et al. (2013) we used a skinned preparation identical to that shown in Fig. 4C (60 min) and Fig. 5, which contained exclusively myosin monomers. We showed that when the preparation was activated directly by Ca^{2+}, no active force developed but full MLC phosphorylation (not different from that observed in intact muscle activated by 10^{-4} M of ACh) was observed (Lan et al., 2013). This suggests that phosphorylation of myosin monomers does not lead to active force development, and that phosphorylation of some of the monomer population in resting intact smooth muscle could explain at least part of the basal phosphorylation seen in virtually all types of smooth muscle. In the process of myosin filament formation, it is likely that a 'critical concentration' of phosphorylated monomers has to be reached before polymerization occurs. This could explain the existence of phosphorylated myosin monomers in intact muscle cells, but by itself it does not offer an explanation for why the monomer phosphorylation is length dependent. The linear decrease in MLC basal phosphorylation with adapted muscle length (Fig. 7C, open symbols) and the linear decrease in myosin monomer concentration with adapted muscle length (Fig. 6) supports the hypothesis that monomers are incorporated into filaments as adapted length increases and thus the pool of phosphorylated, non-force-generating monomeric myosin decreases.

Activation-induced MLC phosphorylation, unlike basal phosphorylation, was correlated with the power output of the muscle, which is an index of the number of working cross-bridges (Mitchell et al., 2001). The finding that activation-induced MLC phosphorylation increases with adapted muscle length, while the basal phosphorylation decreases (Fig. 7C, open symbols), offers further clues as to what the mechanisms for length adaptation may be. The dichotomy of the basal and activation-induced MLC phosphorylation in their dependence on adapted muscle length suggests that there are two pools of myosin in smooth muscle cells, and that the myosin molecules in one pool can be recruited into the other depending on the length at which the muscle is adapted. A recent study from our laboratory (Liu et al., 2013) shows that, unlike

Journal of Cell Science (2017) 130, 2468-2480 doi:10.1242/jcs.202812

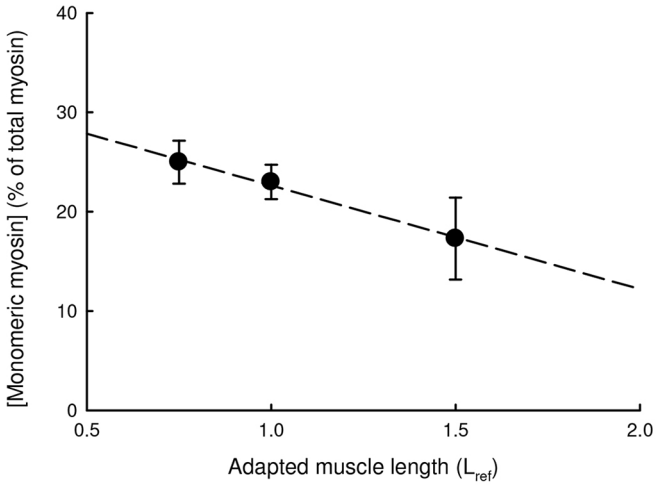

Fig. 6. Concentration of monomeric myosin at each adapted length estimated from the ratio of mm19 staining over maximum of intensity of positive staining when all myosin filaments were assumed to be depolymerized. See Materials and Methods for more details. Data are expressed as means and standard error for each adapted length (n=4). One-way repeated measure ANOVA indicates that there is a statistically significant difference in the amount of monomeric myosin at different adapted lengths (P=0.019). Pairwise multiple comparison (Student–Newman–Keuls method) indicates that at 1.5L_{ref} the concentration of monomeric myosin is less than that at 0.75L_{ref} (P=0.018) and that at L_{ref} (P=0.033). The amount of monomeric myosin at the two shorter lengths, 0.75L_{ref} and 1.0L_{ref}, were not statistically different (P=0.276).

those in striated muscle, myosin filaments in smooth muscles do not have the same length. Rather, the length distribution resembles an exponential decay, with the majority of the filaments being shorter than 0.2 µm (oligomers); many of them are probably myosin dimers. As proposed by Liu et al., myosin polymers and oligomers including dimers act as ratchets and when positioned within the actin filament lattice and activated, can generate force, whereas myosin monomers cannot generate force even if they are within the filament lattice and phosphorylated, because individually they cannot function as ratchets.

Taken together, evidence from the above cited studies and the present study supports a model of smooth muscle containing two interconvertible myosin populations – one residing inside and the other outside the actin filament lattice. The former participates in force generation when the muscle is activated, while the latter does not contribute to force generation regardless of the state of activation. Myosin from the outside pool is recruited into the contractile filament lattice when more contractile units are needed, such as when the muscle is adapted to a longer length. The opposite occurs when the muscle is adapted to a shorter length. Myosin molecules residing outside the contractile filament lattice probably exist in monomeric and oligomeric forms. Myosin polymerization is more likely to occur within the actin filament lattice, due to the existence of actin filament-associated proteins that facilitate myosin filament formation (Seow, 2005 and references within). The compartmentalization may allow the myosin pool outside the contractile units to be relatively free from regulation by the myosin light chain kinase (MLCK) and myosin light chain phosphatase (MLCP) because these enzymes are known to be tethered to actin and myosin filaments in the contractile domain where the myosin filaments reside (Dabrowska et al., 1982; Sellers and Pato, 1984; Trybus, 2000; Smith and Stull, 2000; Sobieszek, 2001; Hatch et al., 2001; Wilson et al., 2002; Mulder et al., 2003, 2004; Surks et al., 2003, 2005; Koga and Ikebe, 2005; Riddick et al., 2008; Hong et al., 2009). The following discussion integrates the present findings to provide support for a simple model (Fig. 8A) that delineates a possible mechanism for length adaptation involving myosin polymerization and depolymerization, as well as migration of myosin in and out of the contractile filament lattice.

Force, velocity and power of muscle adapted to different lengths

As depicted in Fig. 8A, adaptation of smooth muscle cells to different lengths is a process that maximizes the overlap between actin and myosin filaments of a contractile unit. The model is modified from previous models proposed by us (Kuo et al., 2003; Herrera et al., 2005; Liu et al., 2013). A mathematical description of the model was provided by Lambert et al. (2004) detailing the theoretical basis for the length independence of adapted muscle force and linear length dependence of shortening velocity and power output. Maximal overlap between the contractile filaments is achieved by varying the number of contractile units *in series* in proportion to the adapted muscle length. This process is analogous to length adaptation in striated muscle. Farkas and Roussos (1983) have shown that the diaphragm muscle is shorter after experimentally induced emphysema in hamsters without a change in its ability to generate force. This is because in adapting to the shorter length some sarcomeres in the diaphragm muscle of the emphysematous animal have been deleted to restore the maximal overlap of the contractile filaments within the contractile units (sarcomeres). However, the mechanism of length adaptation in smooth muscle is probably different from that of striated muscle because in smooth muscle the adaptation happens over a much shorter period, in a matter of minutes instead of months in striated muscle.

In the model shown in Fig. 8A, the number of contractile units *in parallel* is not altered during length adaptation; the ability of the muscle to generate force is therefore predicted to be unaffected by length adaptation. This is supported by evidence presented in Fig. 2, as well as the finding from a previous study from our laboratory (Kuo et al., 2003). Over a twofold length range, isometric stress was found to be length independent in all muscle preparations used in this study. However, because the number of contractile units in series changes with adapted muscle length according to the model, shortening velocity and power output of the muscle are predicted to be linearly proportional to the muscle length. This is because the overall shortening velocity of a muscle cell is the sum of the shortening velocities of individual contractile units in series, and the overall power output of a muscle cell is the sum of the power outputs of all contractile units within the cell. The model prediction is consistent with our previous findings (Kuo et al., 2003) and with the results shown in Figs 3 and 7 where both V_{max} and P_{max} increase linearly with muscle length.

It should be noted that both shortening velocity and power output are altered to the same extent (by the same scaling factor, see Fig. 3) during length adaptation. The fact that the force–velocity data obtained at short and long (relative to L_{ref}) adapted lengths could be fitted well by scaling the velocity values (without a change in the curvature of the force–velocity curve) is also predicted by the proposed model, which assumes no change in the intrinsic properties of individual contractile units [for further information, see a review by Seow (2013) on the relationship between force–velocity curvature and the intrinsic cross-bridge kinetics].

Journal of Cell Science (2017) 130, 2468-2480 doi:10.1242/jcs.202812

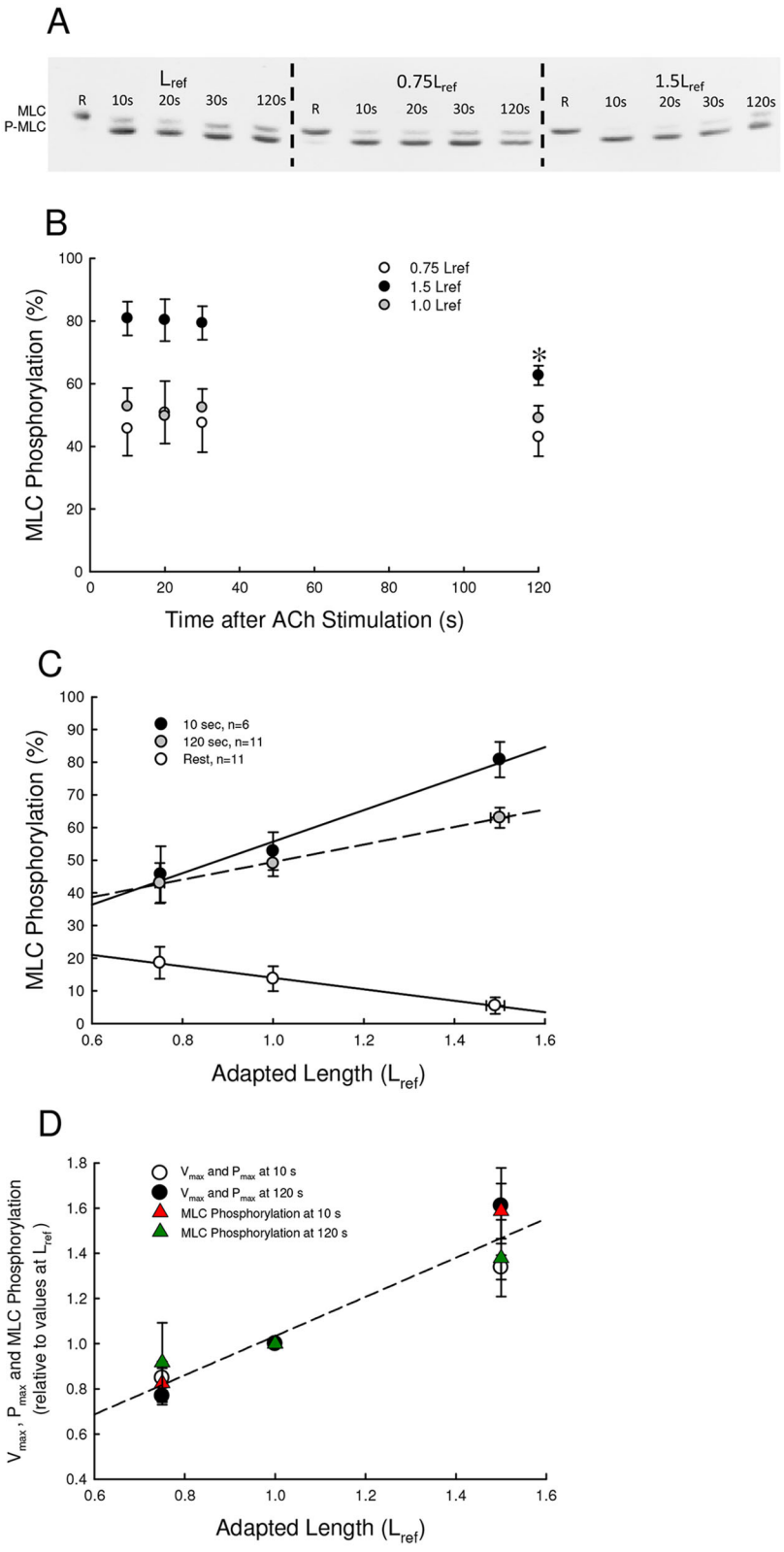

Fig. 7. MLC phosphorylation, shortening velocity and power output at different adapted lengths and times after ACh stimulation. (A) An example of phosphorylated (P-MLC) and non-phosphorylated MLC separated in a 10% glycerol mini-gel. R, resting or basal phosphorylation. (B) MLC phosphorylation as functions of adapted muscle length and time after ACh stimulation. The MLC phosphorylation represents only ACh-induced phosphorylation because the basal phosphorylation was subtracted from the total phosphorylation. Analysis of variance indicates an overall significant difference (P<0.001) among the groups; multiple comparisons revealed significant difference between 1.5 and 0.75L_{ref} (P<0.001), and between 1.5 and 1.0L_{ref} (P<0.001), but no difference between 1.0 and 0.75L_{ref}. There was no interaction between the length groups (P=0.271). *Significant difference from values obtained at 10 and 20 s within the 1.5L_{ref} group (P<0.05, multiple comparison, Student–Newman–Keuls method). n=6 for all data points obtained at 10, 20 and 30 s; n=11 for data points obtained at 0 (rest) and 120 s. n is the number of muscle strips from different animals. (C) MLC phosphorylation as a function of adapted muscle length at different times in contraction. One-way ANOVA for each group indicates significant change in phosphorylation with adapted lengths (P<0.05). n is the number of muscle strips from different animals. (D) V_{max}, P_{max} and MLC phosphorylation at different times after ACh stimulation as functions of adapted muscle length. The relative values within the 0.75L_{ref} group are not different with respect to time (two-way ANOVA, P=0.972) or phosphorylation level (P=0.704) and there is no dependence between the time and phosphorylation groups (P=0.605). The relative values within the 1.5L_{ref} group are also not different with respect to time (P=0.854) or phosphorylation level (P=0.961) and there is no dependence between the time and phosphorylation groups (P=0.180). The data points are therefore grouped together for the linear fit (dashed line), which shows a significant increase with increasing adapted length (P<0.001).

Activation-induced and basal MLC phosphorylation at different adapted muscle lengths

As discussed above, results from force–velocity measurements in the present study (Figs 2, 3 and Fig. 7D) and a previous study from our laboratory (Kuo et al., 2003) are consistent with the model (Fig. 8A). One additional piece of evidence supporting the model came from the present study, i.e. the activation-induced MLC phosphorylation increased linearly with the adapted muscle length and matched quantitatively to the velocity–power data (Fig. 7D). This suggests that a likely explanation for the variation of these three quantities (velocity, power and activation-induced MLC phosphorylation) stems from one common cause, i.e. variation in

Journal of Cell Science (2017) 130, 2468-2480 doi:10.1242/jcs.202812

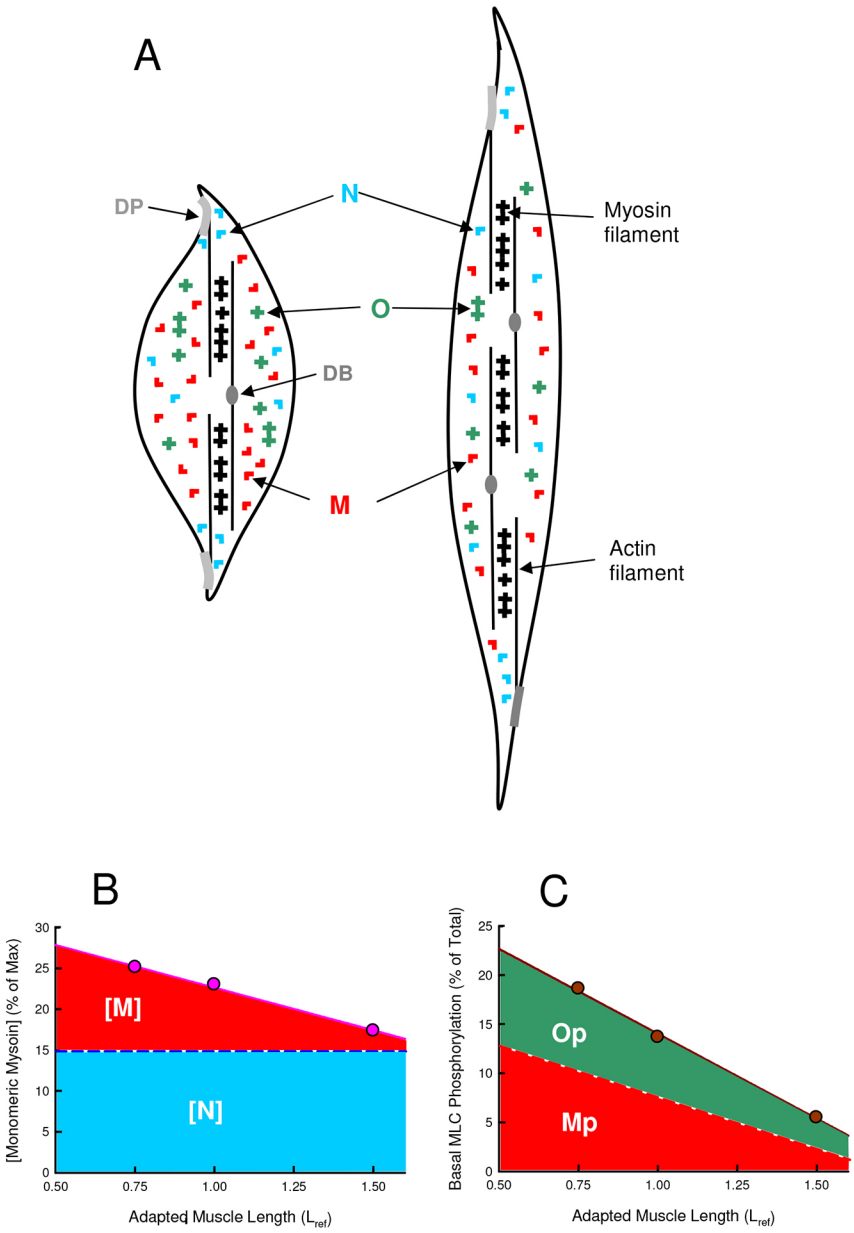

Fig. 8. Modeling of smooth muscle length adaptation. (A) Schematic representation of structural changes associated with reversible adaptation of a smooth muscle cell to long and short lengths. An actin filament lattice consists of actin filaments attached to dense plaques (DP) and dense bodies (DB); a contractile unit consists of a myosin filament sandwiched between two actin filaments and the associated dense bodies or plaques. In this model all contractile units are identical in structure and function. Smooth muscle myosin monomers (M) and oligomers (O) outside the actin filament lattice form a pool of reserve. When adapted to a longer length, the number of contractile units in series is assumed to increase (from two to three in this example), and M and O are recruited from the reserve pool into the newly created actin filament lattice to form filaments. This structural rearrangement results in an increase in shortening velocity and power output in proportion to the adapted length (or the number of contractile units in series) while maintaining the same isometric force. There also is a pool of non-muscle myosins that exist as monomers (N) in the relaxed state. Non-muscle myosins are involved in the formation of membrane-associated actin attachment sites and they do not mix with smooth muscle myosins (Zhang and Gunst, 2017), therefore they are not recruited into the filament lattice to form contractile units (i.e. [N] is independent of length). The mechanism underlying restructuring of actin filament lattice during length adaptation is largely unknown and is not addressed by this model.
(B) Monomeric myosin concentration in relaxed smooth muscle cells as a percentage of total myosin. The pool of monomeric myosins is assumed to be made of M and N, and only the concentration of M is assumed to be length dependent. Note that the concentration of N (15% of total myosin) is an average of two independently published values for airway smooth muscle (see text).
(C) Phosphorylated MLC as a percentage of total MLC in relaxed smooth muscle. The basal phosphorylation is assumed to stem from phosphorylation of some fraction of monomeric (M) and oligomeric (O) myosins in the pool outside the contractile filament lattice (Mp and Op, respectively). The decrease in phosphorylation with increasing length is due to recruitment of M and O into the contractile units where they are dephosphorylated by MLCP in the relaxed state. Non-muscle myosins (N) are assumed to be unphosphorylated in the relaxed state and therefore do not contribute to the basal phosphorylation. See text for a more detailed description of the model.

the number of contractile units in series during length adaptation, as elaborated further below.

It is accepted that phosphorylation of MLC in smooth muscle is required to initiate actomyosin interaction (Kamm and Stull, 1985; Murthy, 2006; Cole and Welsh, 2011). Because MLCK and MLCP are physically associated with the contractile units, it is reasonable to assume that within the contractile units myosin motors are well regulated by these enzymes, i.e. the myosin motors are readily phosphorylated when MLCK is active and MLCP is inactive, and readily dephosphorylated when MLCK is inactive and MLCP is active. However myosin monomers and oligomers outside the contractile units are probably less readily phosphorylated or dephosphorylated as both MLCK and MLCP are less accessible to them, therefore a portion of the monomers and oligomers outside the contractile units may not be phosphorylated when the muscle is activated, and by the same token, they may stay phosphorylated when the muscle is relaxed (therefore, basal phosphorylation). The model (Fig. 8A) therefore assumes that when MLCK is activated, the increase in MLC phosphorylation stems mostly from the myosin motors within the contractile units (as opposed to the myosin outside the contractile domain) due to the proximity of MLCK to its substrate, and this will be accompanied by an increase in the muscle's power output in proportion to the increase in MLC phosphorylation. Furthermore, the level of activation-induced phosphorylation will be higher at longer adapted lengths because of the increased number of contractile units (Fig. 8A) and the shifting of MLCK substrate (myosin) associated with the migration of myosin into the contractile domain. When MLCK is inactivated (during relaxation) the MLCP will probably dephosphorylate the myosin motors within the contractile units more effectively (compared with its action on myosins outside the contractile units), again due to proximity of substrates to the enzyme. The model prediction is consistent with the data shown in Fig. 7C, depicting linear relationships between activation-induced MLC phosphorylation and the adapted muscle length during both early (10 s) and late (120 s) phases of contraction.

Journal of Cell Science (2017) 130, 2468-2480 doi:10.1242/jcs.202812

Because the increased V_{max} and P_{max} observed in muscles adapted to longer lengths is attributed in this model to the increase in the number of in-series contractile units (and the additional filamentous myosin within the units), the model (Fig. 8A) predicts that V_{max}, P_{max} and activation-induced MLC phosphorylation should have the same dependence on the adapted muscle length. This prediction is confirmed by the data presented in Fig. 7D.

In an earlier study it has been shown that a muscle adapted to a longer length consumes more ATP during contraction (Kuo et al., 2003). This is consistent with the model interpretation that the greater extent of activation-induced MLC phosphorylation associated with longer adapted lengths, and the accompanied increase in the ability of the muscle to do work (and consume energy) is due to an increase in the number of contractile units, and not due to an increase in the muscle's energetic efficiency.

To explain the linear decrease of basal MLC phosphorylation with adapted muscle length (Fig. 7C, open symbols) and its possible connection to the linear decrease of myosin monomer concentration with adapted muscle length (Fig. 6) we developed a mathematical model. To simplify the model, three assumptions were made: (1) the myosin pool inside the contractile filament lattice consists of smooth muscle myosin polymers and oligomers, whereas the pool outside the lattice consists of smooth muscle myosin monomers (M) and oligomers (O), and non-muscle myosin monomers (N) (Fig. 8A); (2) non-muscle myosin exists as non-phosphorylated monomers in the relaxed state and, unlike smooth muscle monomers and oligomers, they do not migrate into or out of the contractile units during length adaptation [as shown by Zhang and Gunst (2017), they polymerize when activated and are essential in the formation of membrane adhesome complexes; they do not mix with smooth muscle myosin]; and (3) basal phosphorylation stems from phosphorylation of a fraction of smooth muscle monomeric and oligomeric myosin outside the contractile units in the relaxed state. As a consequence of the assumptions, the concentration of non-muscle myosin monomers is independent of the adapted muscle length (Fig. 8B). There are two studies in which the concentration of non-muscle myosin in airway smooth muscle was measured (Halayko et al., 1996; Zhang and Gunst, 2017). We took the average (∼15%) of their measurements (11.4 and 18.7%) and used it as the fractional concentration of non-muscle myosin (percentage to total myosin) in our model. Because the mm19 antibody recognizes both smooth muscle and non-muscle myosin monomers (Ikebe et al., 2001), the non-muscle myosin monomer concentration (which is length independent according to assumption 2) is subtracted from the estimated total myosin monomer concentration (Fig. 6) to obtain the smooth muscle myosin monomer concentration (red area, Fig. 8B). A linear fit of the data shows that the estimated concentration of smooth muscle myosin monomers (M) and its dependence on muscle length is: $M(L)=18-10.4L$, where L is the muscle length as a fraction of L_{ref}.

To explain the linear decrease in basal phosphorylation with adapted muscle length (Fig. 7C) we rely on assumption 3, which stipulates that the observed phosphorylation represents a fraction of the total myosin pool outside the contractile units. From Fig. 7D, doubling the adapted length results in ∼70% increase in activation-induced MLC phosphorylation with concomitant increases in shortening velocity and power output, indicating a ∼70% increase in the pool of myosin inside the contractile units and a corresponding decrease in the pool outside the contractile units. Because the decrease in basal MLC phosphorylation from 0.75 to $1.5L_{ref}$ is 13.1% (Fig. 7C, open symbols), the fraction of phosphorylated myosin (outside pool) in the relaxed state is estimated to be 13.1/70=0.187, or 18.7% of the outside pool. We can further deduce that the 18.7% is made up of two components: phosphorylated smooth muscle myosin monomers (Mp) and phosphorylated smooth muscle myosin oligomers (Op) (Fig. 8C). We do not have information for the fraction of phosphorylated M, but we assume Mp is proportional to M, i.e. $Mp=fM$, where f is a constant of proportionality. $f=0$ and $f=1$ denote zero or full phosphorylation of M in the relaxed state, respectively. Fig. 8C shows Mp (red area) as a function of muscle length when $f=1$, with the remaining basal phosphorylation attributed to the phosphorylation of smooth muscle oligomeric myosin (O). The model cannot specify the exact proportions corresponding to Mp and Op, because f is not known. The linear fit for the total basal phosphorylation (T) as a function of the adapted muscle length is: $T(L)=31.4-17.3L$. Therefore $Op=T(L)-fM(L)$.

Clearly the model has several limitations. Firstly, the mm19 immunohistochemical staining is a semi-quantitative measure of the concentration of myosin monomers; the model parameters derived from the concentration estimation are therefore semi-quantitative. Secondly, the assumptions upon which the model is based are supported mostly by indirect evidence, and their validity requires verification.

Relation to early studies

Muscle length dependence of MLC phosphorylation has been investigated previously in smooth muscle (Hai, 1991; Washabau et al., 1991; Wingard et al., 1995; Mehta et al., 1996; Szeto and Hai, 1996). At first glance, the present study appears to be just a repeat of the previous studies. Although measurements of MLC phosphorylation in the cited studies were carried out at different muscle lengths, muscle preparations used in those experiments had not been adapted (or at least not fully adapted) to each length before the measurements were made. As a result, besides finding length-dependent differences in MLC phosphorylation, they also found that active force was dependent on muscle length. In contrast, our measurements were conducted in length-adapted muscle where active force was length independent (Fig. 2). The present study also includes estimation of myosin monomer concentration, shortening velocity and power output of the muscle as functions of both adapted length, and the extent of MLC phosphorylation at two time points during an isometric contraction; only the combination of such data could allow interpretation of our observations in terms of possible subcellular structural change and its consequence on muscle performance.

It is interesting to note that length change per se does not determine the extent of MLC phosphorylation in the absence of length adaptation. Mehta et al. (1996) showed that in a muscle activated at an optimal length and abruptly shortened to half of that length, there was no change in MLC phosphorylation immediately after the length change, despite a large decrease in active force.

It has been observed in tracheal smooth muscle that tyrosine phosphorylation (stimulated by acetylcholine) of focal adhesion kinase (FAK) and paxillin is associated with length-dependent MLC phosphorylation (Tang and Gunst, 2001). Because FAK and paxillin phosphorylation is important in cytoskeletal remodelling during length adaptation involving rearrangement of contractile units, the observation is consistent with our model (Fig. 8) that length adaptation underlies length-dependent MLC phosphorylation. Adaptation of the cytoskeleton to different cell lengths is another important aspect of smooth muscle length adaptation. This aspect of adaptation is not addressed in the present study because it requires a different set of methodological

approaches. A recent study by Zhang and Gunst (2017) demonstrated that phosphorylation of the heavy and light chains of non-muscle myosin is important in the reorganization of cortical actin cytoskeleton.

Alternative explanations

An alternative explanation for the length-dependent phosphorylation is that the enzymes involved in regulating the level of MLC phosphorylation (i.e. MLCK and MLCP) are themselves regulated by the muscle cell length. Specifically one would have to assume that there are antagonistic functions of MLCK and MLCP and they are modulated by cell length in such a way that gives rise to the dichotomy of MLC phosphorylation in the relaxed and activated states at different muscle lengths (Fig. 7C). Although physical stretch is known to induce intracellular calcium release in smooth muscle cells (Nakayama and Tanaka, 1993), this could explain the observed increase in activation-induced MLC phosphorylation at longer muscle length; it does not explain the existence of basal phosphorylation without active force generation and the linear decrease in basal phosphorylation with adapted length (Fig. 7C). Another possible explanation is that accessibility of myosin to MLCK and MLCP is altered at different cell lengths. Specifically, a greater access to their substrates by the enzymes is achieved at a longer cell length. This, however, contradicts the observation that without length adaptation the basal level of MLC phosphorylation is length insensitive (Washabau et al., 1991; Wingard et al., 1995). This alternative model also cannot explain the existence of basal phosphorylation in the absence of active force. Yet another possible explanation, as mentioned earlier, is that there is a threshold of MLC phosphorylation that must be exceeded before the cyclical interaction of actomyosin can proceed (Warshaw et al., 1990; Rembold et al., 2004). This, however, does not explain why there is basal phosphorylation in the first place. It should be pointed out that all the alternative explanations are not mutually exclusive of the explanation we propose, as summarized in Fig. 8.

Conclusion

Adaptation of smooth muscle to different lengths is accompanied by length-proportional changes in shortening velocity, power output and activation-induced MLC phosphorylation, and is inversely proportional to MLC basal phosphorylation and the concentration of myosin monomers. These observations can be explained by a simple model where myosin monomers and filaments interconvert and migrate to different subcellular domains depending on the length at which the muscle is adapted.

MATERIALS AND METHODS

Muscle preparation

Sheep tracheal smooth muscle preparations were used. Sheep tracheas were obtained from a local abattoir. All experimental procedures were approved by the Ethics Committee for Animal Care and the Biosafety Committee of the University of British Columbia and conformed to the guidelines set out by the Canadian Council on Animal Care.

The tissues were transported from the slaughterhouse to our laboratory in ice-cold physiological saline solution (PSS) of the following composition: 118 mM NaCl, 4 mM KCl, 1.2 mM NaH_2PO_4, 22.5 mM $NaHCO_3$, 2 mM $MgSO_4$, 2 mM $CaCl_2$ and 2 g/l dextrose at pH 7.4. Some tissues were immediately used in experiments; some were stored in PSS at 4°C and used on subsequent days for up to 4 days. Smooth muscle strips (5–7 mm long, 1.5–2 mm wide, 0.2–0.3 mm thick) were dissected from the tracheas and aluminum foil clips were affixed to both ends of the strip for attachment to the force/length transducer (duo mode, model 300C, Aurora Scientific, Aurora, ON, Canada). Strips were mounted at their *in situ* length and equilibrated in the presence of 5×10^{-5} M indomethacin for 60 min in order to abolish spontaneous intrinsic tone. To ensure that the muscle preparations used in experiments were viable and generating a normal amount of force, the preparations were periodically activated isometrically (once every 5 min for 10 s) by electric field stimulation (EFS) (60 Hz, 15 V, and a current density sufficient to elicit maximal response from the muscle) at the *in situ* length and kept in PSS at 37°C and aerated with carbogen (95% O_2 and 5% CO_2). The muscle strips were considered equilibrated when the isometric force reached a steady maximal value. The *in situ* length of the muscle was used as a reference length (L_{ref}) for normalization of length and velocity measurements.

Skinned muscle preparation

This muscle preparation was used as a positive control for our immunohistochemical staining of monomeric myosin. Exposure of myosin filaments to high concentrations of ATP and EGTA at 200 mM ionic strength causes the filaments to disassemble into monomers (Cande et al., 1983; Lan et al., 2013). Intact trachealis strips were periodically activated at L_{ref} by EFS as described above to ensure that the isometric force reached a steady maximal value. After this equilibration procedure, the strips were soaked in skinning solution at room temperature (1% Triton X-100, 5 mM ATP, 2 mM EGTA, 1 mM $MgCl_2$, 10 mM imidazole and sufficient KCl to ensure an ionic strength of 200 mM for the solution, pH 7.0 at room temperature) for different time periods. The skinned preparations were then fixed for immunohistochemistry and electron microscopy.

Immunohistochemistry and quantification of myosin monomer concentration

Four tracheas were used for this analysis. Muscle strips were adapted to 0.75, 1.0 and 1.5L_{ref} as described above. At the final adapted length, the muscle strips were fixed at 37°C in 10% formalin under resting conditions. The fixed strips were embedded in paraffin. Two cross-sections were obtained from each muscle strip. These sections were 4 µm thick and approximately 100 µm apart along the long axis of the muscle strip. The sections were loaded onto the BOND-RX automated immunostaining machine (Leica Biosystems). After dewaxing, antigen retrieval was performed with heat in 10 mM sodium citrate buffer at pH 6.0. mm19 antibody, an IgG class mouse monoclonal antibody produced against chicken gizzard smooth muscle myosin monomer (Ikebe et al., 2001) was used at 1:1000 dilution to label monomeric myosin in the sections. The antibody interacts with smooth muscle myosin at the tail end and prevents filament formation. It dissolves filaments and also prevents filament formation when the antibody is added to monomeric myosin (Ikebe et al., 2001). This same antibody was used by Milton et al. (2011) and through confocal microscopy they were able to separate filamentous from monomeric myosin, demonstrating relative specificity for myosin monomers; however, weak affinity for myosin filaments cannot be excluded. Signal detection was by a biotin-free, polymeric alkaline phosphatase (AP)-linker antibody conjugate system optimized for the BOND-RX. The substrate chromogen, Fast Red, identified the antibody–antigen complex via a red precipitate. Hematoxylin counterstaining allowed visualization of cell nuclei (blue).

Coverslips were applied to the stained sections. After air drying for 24 h, the slides were scanned with an Aperio ScanScope XT brightfield scanner (Leica Biosystems). The scanner digitized the whole microscope slides at 40× magnification and provided resolution up to 0.25 µm/pixel. The degree of monomeric myosin staining in the muscle bundles was quantified using an image-viewer Aperio ImageScope (Leica Biosystems). Regions of interest for analysis were chosen as the entire cross-section of the muscle tissue, excluding blood vessels, glands, and loose connective tissue around the muscle cell bundles. A color segmentation algorithm was applied to all the sections. Total intensity of positive mm19 staining was normalized by the total number of pixels within the region of interest to estimate the concentration of monomeric myosin on each section. The mean value of both sections from the same muscle strip was used to represent the concentration of monomeric myosin of that particular muscle strip. To convert the intensity of staining to concentration as a percentage of total myosin, a calibration curve was generated. The average staining for negative controls where the primary antibody was omitted was taken as 0%, and the average maximal intensity of staining, which was found in our positive

Journal of Cell Science (2017) 130, 2468-2480 doi:10.1242/jcs.202812

controls (skinned muscle cells exposed to depolymerizing agents ATP and EGTA at 200 mM ionic strength), was taken as 100%. The calibration curve allowed us to convert the staining intensity observed in intact muscles to monomer concentration as a percentage of maximal concentration.

Electron microscopy

Primary fixation of tissue (15 min) was carried out while the muscle strips were still attached to the force transducer at its *in situ* length. The fixing solution contained the following: 1% paraformaldehyde, 2.5% glutaraldehyde and 2% tannic acid in 0.1 M sodium cacodylate buffer. The fixing solution was kept at room temperature during primary fixation. After primary fixation, the muscle strip was removed from the apparatus and cut into small blocks (~2 mm by ~0.5 mm by ~0.2 mm in dimension) in cold fixation buffer and kept in the same fixative for 2 h at 4°C on a shaker. For secondary fixation the tissue blocks were transferred to 1% osmium buffer for 1.5 h at 4°C on the shaker, followed by three washes with distilled water (10 min per wash). The tissue blocks were then stained with 1% uranyl acetate, dehydrated with increasing concentrations of ethanol (50, 70, 80, 90, 95 and 100%) and finally with propylene oxide. After dehydration, small tissue pieces were embedded in resin (TAAB 812 mix). The resin blocks were sectioned with a diamond knife to obtain ultra-thin sections 60 nm in thickness. The sections (on copper grids) were further stained with 1% uranyl acetate and lead citrate. Images of cross-sections of the muscle cells were obtained with an electron microscope (Philips/FEI Tecnai 12 TEM) equipped with a digital camera (Gatan 792) at a magnification of 37,000×. To capture the whole cross-section of a single cell it often required taking multiple images of different parts of a cell cross-section, and merging the parts together using Adobe Photoshop.

Measurement of MLC phosphorylation

Muscle strips frozen under the experimental conditions described above were used for determination of the extent of MLC phosphorylation. Acetone was pre-chilled at dry-ice temperature (−78.5°C). The tissue strips were snap-frozen in the pre-chilled acetone while it was still attached to the measurement apparatus. Frozen strips were quickly taken off the apparatus and placed in tubes of pre-chilled acetone containing 5% trichloroacetic acid (TCA) and 10 mM dithiothreitol (DTT) and stored at −80°C. Within a week the strips were processed to extract total protein. Immediately before the assay, the strips were brought to room temperature. TCA was removed from the strips by submerging them in two washes (30 min each) of 1 ml acetone containing 10 mM DTT. At a proportion of 150 µl/mg wet tissue weight, the strip was then homogenized in lysis buffer containing 6.4 M urea, 5 mM DTT, 10 mM EGTA, 1 mM EDTA, 5 mM NaF, 1 mM phenylmethylsulfonyl fluoride, 26.4 mM Tris base and 29.3 mM glycine. Sample tubes were mounted on a rotator at 4°C, inverted continually for 2 h, and then centrifuged at 13,200 ***g*** for 30 min at 4°C. The supernatant was obtained immediately after centrifugation and the Biorad QuickStart Bradford protein assay was performed to obtain total protein concentration for each sample. An aliquot of each supernatant was then diluted further with additional lysis buffer containing 0.02% Bromophenol Blue and stored at −80°C.

Phosphorylated and non-phosphorylated MLC were separated on a 10% acrylamide–40% glycerol mini gel with 3% acrylamide-urea stacking gel. Protein extracted from each individual muscle strip, which represented a snapshot of a specific time point at an adapted muscle length, was loaded into an individual lane without sample pooling. Electrophoresis was performed at 200 V for 2.5 h at room temperature in running buffer containing 100 mM glycine, 50 mM Tris and β-mercaptoethanol (1 ml/l buffer). An additional 0.5 ml of β-mercaptoethanol was added to the inner chamber. Proteins were then transferred to 0.2 µm nitrocellulose membrane at 25 V at 4°C overnight. Non-specific binding sites were blocked with Tris-base saline (TBS) with 5% bovine serum albumin (BSA) for 1 h at room temperature. Western immunoblots were developed using, in sequence, a monoclonal mouse antibody to smooth muscle MLC (Sigma, clone MY-21; 1:5000) and goat anti-mouse IRDye 800-conjugated antibody (Rockland, cat. no. 610-132-121; 1:10,000) in TBST (Tween) with 5% BSA. The membranes were washed three times with TBST for 10 min each time during standard washing steps, i.e. after primary and secondary antibodies. The membrane was then scanned on a LI-COR Odyssey 2.1 infrared imaging system. The intensity of each band was analyzed using the software Odyssey 2.1 with background intensity subtracted from the total integrated optical intensity. Fractional phosphorylation in each sample was determined as the ratio of the optical density of the band containing phosphorylated light chain (the lower band) to the sum of the density of the bands containing phosphorylated and non-phosphorylated proteins (the lower and upper bands, respectively) in the same lane.

Experimental procedures for determining muscle mechanical properties and MLC phosphorylation

From each trachea we isolated three strips for mechanical experiments and 15 strips for measurement of MLC phosphorylation. All strips were equilibrated at L_{ref}. After stable maximal isometric force was achieved, the strips were divided into three groups; the muscle length was set to $0.75L_{ref}$ in one group and $1.5L_{ref}$ in the second group, and in the third group the length was kept at L_{ref}. After each length change, the strip was subjected to the process of length adaptation in which it was stimulated by EFS to produce a brief (10 s) isometric contraction once every 5 min until the isometric force recovered to approximately the same level as it was before the length change (Wang et al., 2001); this process normally took 25–30 min, i.e. five to six cycles of contraction/relaxation. The three strips used for mechanical experiments were then stimulated with 3×10^{-5} M ACh to elicit isometric contraction. Fig. 1A shows recordings of isometric force development after ACh stimulation. Force–velocity properties of the muscle were assessed at two time points, 10 and 120 s after stimulation by ACh by applying isotonic quick releases and measuring the shortening velocity 0.1 s after the quick release (Fig. 1B and C). The slope at 0.1 s after the release was obtained by a linear fit to the length data points 0.08–0.12 s after the quick release. The sampling rate was 200 Hz. The 0.1 s delay was allowed to avoid distortion of velocity measurements by the recoil of the series viscoelastic element of muscle preparation. At each time point, the quick release was performed five times with five different isotonic loads applied in random orders: 10, 15, 25, 50 and 75% of the maximal active force (F_{max}) produced by ACh stimulation. After each quick release, the muscle was rinsed repeatedly with fresh PSS to relax the muscle and to return force to its resting level. Subsequent ACh stimulation was performed at least 20 min after a previous stimulation. The measured velocity values were plotted against the corresponding isotonic loads and the data were fitted with the Hill equation of the form: $(F+a)(V+b)=c$, where F is the isotonic force, V is the shortening velocity and a, b and c are constants. A non-linear least-squares fit to the data was performed using SigmaPlot 11.0. Fitting of the Hill equation was only done for the data obtained at L_{ref}. For force–velocity data obtained at 0.75 and $1.5L_{ref}$, the curve that fitted the L_{ref} data was scaled down and up, respectively, by multiplying the velocity values by a constant (scaling factor) to fit the data with a non-linear least-squares method from SigmaPlot 11.0. The force–power curve was obtained from the force–velocity curve by multiplying force and velocity values, because power=force×velocity, i.e. $P=F\times V=F[c/(F+a)-b]$. The maximal value of the power function is designated as P_{max}.

The levels of MLC phosphorylation were measured at three different adapted lengths (0.75, 1.0 and 1.5 L_{ref}) and at four time points (10, 20, 30 and 120 s after stimulation by ACh); note that force–velocity properties were measured at only two time points (10 and 120 s). At each length, five muscle strips were used; four strips designated for determining MLC phosphorylation after ACh (3×10^{-5} M) stimulation were frozen at the four time points during contraction, and the fifth one from the same trachea was frozen in the relaxed state for determination of baseline phosphorylation. All five strips were adapted to the same length (0.75, 1.0 or $1.5L_{ref}$) using the same adaptation protocol. A complete set of phosphorylation experiments therefore consisted of 15 strips from the same trachea, adapted to three different lengths. Two additional control strips were equilibrated in the absence of indomethacin and frozen at L_{ref} at rest and 120 s after administration of 3×10^{-5} M ACh. Results from the additional control strips showed no difference from the regular control (i.e. in the presence of indomethacin) and are not reported in the Results section.

Statistical analysis

Results obtained at different adapted muscle lengths were compared using one-way and two-way ANOVA, as well as one-way repeated measures ANOVA and two-way repeated measures ANOVA, all with *post hoc* analyses. Means and standard errors are plotted in the graphs and reported in the text. A P value of 0.05 or less was used to reject the null hypothesis.

Acknowledgements

Special thanks are due to Meadow Valley Meats Limited (Pitt Meadows, BC) for the supply of fresh sheep tracheas in kind support for this research project.

Competing interests

The authors declare no competing or financial interests.

Author contributions

Conceptualization: P.C., L.W., P.D.P., C.Y.S.; Methodology: P.C., L.W., G.Y.Y.T., M.I., P.D.P., C.Y.S.; Software: C.Y.S.; Validation: P.C., L.W., G.Y.Y.T., M.I., P.D.P., C.Y.S.; Formal analysis: P.C., L.W., G.Y.Y.T., P.D.P., C.Y.S.; Investigation: P.C., L.W., G.Y.Y.T., P.D.P., C.Y.S.; Resources: M.I., P.D.P., C.Y.S.; Data curation: P.C., L.W.; Writing – original draft: P.C., L.W., C.Y.S.; Writing – review and editing: P.C., L.W., M.I., P.D.P., C.Y.S.; Supervision: C.Y.S.; Project administration: C.Y.S.; Funding acquisition: P.D.P., C.Y.S.

Funding

This work was supported by a Discovery Grant from the Natural Sciences and Engineering Research Council of Canada.

References

Abe, Y., Kasuya, Y., Kudo, M., Yamashita, K., Goto, K., Masaki, T. and Takuwa, Y. (1991). Endothelin-1-induced phosphorylation of the 20-kDa myosin light chain and caldesmon in porcine coronary artery smooth muscle. *Jpn. J. Pharmacol.* **57**, 431-435.

Adam, L. P., Milio, L., Brengle, B. and Hathaway, D. R. (1990). Myosin light chain and caldesmon phosphorylation in arterial muscle stimulated with endothelin-1. *J. Mol. Cell Cardiol.* **22**, 1017-1023.

Bai, T. R., Bates, J. H., Brusasco, V., Camoretti-Mercado, B., Chitano, P., Deng, L. H., Dowell, M., Fabry, B., Ford, L. E., Fredberg, J. J. et al. (2004). On the terminology for describing the length-force relationship and its changes in airway smooth muscle. *J. Appl. Physiol.* **97**, 2029-2034.

Bursac, P., Lenormand, G., Fabry, B., Oliver, M., Weitz, D. A., Viasnoff, V., Butler, J. P. and Fredberg, J. J. (2005). Cytoskeletal remodelling and slow dynamics in the living cell. *Nat. Mater.* **4**, 557-561.

Cande, W. Z., Tooth, P. J. and Kendrick-Jones, J. (1983). Regulation of contraction and thick filament assembly-disassembly in glycerinated vertebrate smooth muscle cells. *J. Cell. Biol.* **97**, 1062-1071.

Chen, C., Krishnan, R., Zhou, E., Ramachandran, A., Tambe, D., Rajendran, K., Adam, R. M., Deng, L. and Fredberg, J. J. (2010). Fluidization and resolidification of the human bladder smooth muscle cell in response to transient stretch. *PLoS ONE* **5**, e12035.

Chitano, P., Worthington, C. L., Jenkin, J. A., Stephens, N. L., Gyapong, S., Wang, L. and Murphy, T. M. (2005). Ontogenesis of myosin light chain phosphorylation in guinea pig tracheal smooth muscle. *Pediatr. Pulmonol.* **39**, 108-116.

Cole, W. C. and Welsh, D. G. (2011). Role of myosin light chain kinase and myosin light chain phosphatase in the resistance arterial myogenic response to intravascular pressure. *Arch. Biochem. Biophys.* **510**, 160-173.

Dabrowska, R., Hinkins, S., Walsh, M. P. and Hartshorne, D. J. (1982). The binding of smooth muscle myosin light chain kinase to actin. *Biochem. Biophys. Res. Commun.* **107**, 1524-1531.

Deng, L., Trepat, X., Butler, J. P., Millet, E., Morgan, K. G., Weitz, D. A. and Fredberg, J. J. (2006). Fast and slow dynamics of the cytoskeleton. *Nat. Mater.* **5**, 636-640.

Ekmehag, B. L. and Hellstrand, P. (1989). Shortening velocity, myosin light chain phosphorylation and Ca^{2+} dependence of force during metabolic inhibition in smooth muscle of rat portal vein. *Acta. Physiol. Scand.* **136**, 367-376.

Fabry, B. and Fredberg, J. J. (2003). Remodeling of the airway smooth muscle cell: are we built of glass? *Respir. Physiol. Neurobiol.* **137**, 109-124.

Farkas, G. A. and Roussos, C. (1983). Diaphragm in emphysematous hamsters: sarcomere adaptability. *J. Appl. Physiol. Respir. Environ. Exerc. Physiol.* **54**, 1635-1640.

Fischer, W. and Pfitzer, G. (1989). Rapid myosin phosphorylation transients in phasic contractions in chicken gizzard smooth muscle. *FEBS Lett.* **258**, 59-62.

Frearson, N., Focant, B. W. and Perry, S. V. (1976). Phosphorylation of a light chain component of myosin from smooth muscle. *FEBS Lett.* **63**, 27-32.

Gerthoffer, W. T. and Murphy, R. A. (1983). Myosin phosphorylation and regulation of cross-bridge cycle in tracheal smooth muscle. *Am. J. Physiol.* **244**, C182-C187.

Gunst, S. J. and Fredberg, J. J. (2003). The first three minutes: smooth muscle contraction, cytoskeletal events, and soft glasses. *J. Appl. Physiol.* **95**, 413-425.

Gunst, S. J. and Wu, M. F. (2001). Selected contribution: plasticity of airway smooth muscle stiffness and extensibility: role of length-adaptive mechanisms. *J. Appl. Physiol.* **90**, 741-749.

Gunst, S. J., Meiss, R. A., Wu, M. F. and Rowe, M. (1995). Mechanisms for the mechanical plasticity of tracheal smooth muscle. *Am. J. Physiol.* **268**, C1267-C1276.

Hai, C.-M. (1991). Length-dependent myosin phosphorylation and contraction of arterial smooth muscle. *Pflugers Arch.* **418**, 564-571.

Halayko, A. J., Salari, H., Ma, X. and Stephens, N. L. (1996). Markers of airway smooth muscle cell phenotype. *Am. J. Physiol.* **270**, L1040-L1051.

Hatch, V., Zhi, G., Smith, L., Stull, J. T., Craig, R. and Lehman, W. (2001). Myosin light chain kinase binding to a unique site on F-actin revealed by three-dimensional image reconstruction. *J. Cell Biol.* **154**, 611-618.

Hathaway, D. R. and Haeberle, J. R. (1985). A radioimmunoblotting method for measuring myosin light chain phosphorylation levels in smooth muscle. *Am. J. Physiol.* **249**, C345-C351.

Herrera, A. M., McParland, B. E., Bienkowska, A., Tait, R., Paré, P. D. and Seow, C. Y. (2005). 'Sarcomeres' of smooth muscle: functional characteristics and ultrastructural evidence. *J. Cell Sci.* **118**, 2381-2392.

Hong, F., Haldeman, B. D., John, O. A., Brewer, P. D., Wu, Y.-Y., Ni, S., Wilson, D. P., Walsh, M. P., Baker, J. E. and Cremo, C. R. (2009). Characterization of tightly associated smooth muscle myosin-myosin light-chain kinase-calmodulin complexes. *J. Mol. Biol.* **390**, 879-892.

Horowitz, A., Trybus, K. M., Bowman, D. S. and Fay, F. S. (1994). Antibodies probe for folded monomeric myosin in relaxed and contracted smooth muscle. *J. Cell Biol.* **126**, 1195-1200.

Huang, Y., Day, R. N. and Gunst, S. J. (2014). Vinculin phosphorylation at tyr1065 regulates vinculin conformation and tension development in airway smooth muscle tissues. *J. Biol. Chem.* **289**, 3677-3688.

Ikebe, M., Onishi, H. and Watanabe, S. (1977). Phosphorylation and dephosphorylation of a light chain of the chicken gizzard myosin molecule. *J. Biochem.* **82**, 299-302.

Ikebe, M., Komatsu, S., Woodhead, J. L., Mabuchi, K., Ikebe, R., Saito, J., Craig, R. and Higashihara, M. (2001). The tip of the coiled-coil rod determines the filament formation of smooth muscle and nonmuscle myosin. *J. Biol. Chem.* **276**, 30293-30300.

Ishii, N. and Takahashi, K. (1982). Length-tension relation of single smooth muscle cells isolated from the pedal retractor muscle of *Mytilus edulis*. *J. Muscle Res. Cell Motil.* **3**, 25-38.

Kamm, K. E. and Stull, J. T. (1985). The function of myosin and myosin light chain kinase phosphorylation in smooth muscle. *Annu. Rev. Pharmacol. Toxicol.* **25**, 593-620.

Koga, Y. and Ikebe, M. (2005). p116Rip decreases myosin II phosphorylation by activating myosin light chain phosphatase and by inactivating RhoA. *J. Biol. Chem.* **280**, 4983-4991.

Kuo, K.-H., Herrera, A. M., Wang, L., Paré, P. D., Ford, L. E., Stephens, N. L. and Seow, C. Y. (2003). Structure-function correlation in airway smooth muscle adapted to different lengths. *Am. J. Physiol. Cell Physiol.* **285**, C384-C390.

Lambert, R. K., Paré, P. D. and Seow, C. Y. (2004). Mathematical description of geometric and kinematic aspects of smooth muscle plasticity and some related morphometrics. *J. Appl. Physiol.* **96**, 469-476.

Lan, B., Wang, L., Zhang, J., Pascoe, C. D., Norris, B. A., Liu, J. C.-Y., Solomon, D., Paré, P. D., Deng, L. and Seow, C. Y. (2013). Rho-kinase mediated cytoskeletal stiffness in skinned smooth muscle. *J. Appl. Physiol.* **115**, 1540-1552.

Liu, J. C.-Y., Rottler, J., Wang, L., Zhang, J., Pascoe, C. D., Lan, B., Norris, B. A., Herrera, A. M., Paré, P. D. and Seow, C. Y. (2013). Myosin filaments in smooth muscle cells do not have a constant length. *J. Physiol.* **591**, 5867-5878.

Mehta, D., Wu, M. F. and Gunst, S. J. (1996). Role of contractile protein activation in the length-dependent modulation of tracheal smooth muscle force. *Am. J. Physiol.* **270**, C243-C252.

Mehta, D., Wang, Z., Wu, M. F. and Gunst, S. J. (1998). Relationship between paxillin and myosin phosphorylation during muscarinic stimulation of smooth muscle. *Am. J. Physiol.* **274**, C741-C747.

Milton, D. L., Schneck, A. N., Ziech, D. A., Ba, M., Facemyer, K. C., Halayko, A. J., Baker, J. E., Gerthoffer, W. T. and Cremo, C. R. (2011). Direct evidence for functional smooth muscle myosin II in the 10S self-inhibited monomeric conformation in airway smooth muscle cells. *Proc. Natl. Acad. Sci. USA* **108**, 1421-1426.

Mitchell, R. W., Seow, C. Y., Burdyga, T., Maass-Moreno, R., Pratusevich, V. R., Ragozzino, J. and Ford, L. E. (2001). Relationship between myosin phosphorylation and contractile capability of canine airway smooth muscle. *J. Appl. Physiol.* **90**, 2460-2465.

Mulder, J., Poland, M., Gebbink, M. F. B. G., Calafat, J., Moolenaar, W. H. and Kranenburg, O. (2003). p116Rip is a novel filamentous actin-binding protein. *J. Biol. Chem.* **278**, 27216-27223.

Mulder, J., Ariaens, A., van den Boomen, D. and Moolenaar, W. H. (2004). p116Rip targets myosin phosphatase to the actin cytoskeleton and is essential for RhoA/ROCK-regulated neuritogenesis. *Mol. Biol. Cell* **15**, 5516-5527.

Murthy, K. S. (2006). Signaling for contraction and relaxation in smooth muscle of the gut. *Annu. Rev. Physiol.* **68**, 345-374.
Nakayama, K. and Tanaka, Y. (1993). Stretch-induced contraction and Ca^{2+} mobilization in vascular smooth muscle. *Biol. Signals* **2**, 241-252.
Opazo Saez, A., Zhang, W., Wu, Y., Turner, C. E., Tang, D. D. and Gunst, S. J. (2004). Tension development during contractile stimulation of smooth muscle requires recruitment of paxillin and vinculin to the membrane. *Am. J. Physiol. Cell Physiol.* **286**, C433-C447.
Pratusevich, V. R., Seow, C. Y. and Ford, L. E. (1995). Plasticity in canine airway smooth muscle. *J. Gen. Physiol.* **105**, 73-94.
Ratz, P. H., Hai, C. M. and Murphy, R. A. (1989). Dependence of stress on cross-bridge phosphorylation in vascular smooth muscle. *Am. J. Physiol.* **256**, C96-C100.
Rembold, C. M., Wardle, R. L., Wingard, C. J., Batts, T. W., Etter, E. F. and Murphy, R. A. (2004). Cooperative attachment of cross bridges predicts regulation of smooth muscle force by myosin phosphorylation. *Am. J. Physiol. Cell Physiol.* **287**, C594-C602.
Riddick, N., Ohtani, K. and Surks, H. K. (2008). Targeting by myosin phosphatase-RhoA interacting protein mediates RhoA/ROCK regulation of myosin phosphatase. *J. Cell Biochem.* **103**, 1158-1170.
Sellers, J. R. and Pato, M. D. (1984). The binding of smooth muscle myosin light chain kinase and phosphatases to actin and myosin. *J. Biol. Chem.* **259**, 7740-7746.
Seow, C. Y. (2005). Myosin filament assembly in an ever-changing myofilament lattice of smooth muscle. *Am. J. Physiol. Cell Physiol.* **289**, C1363-C1368.
Seow, C. Y. (2013). Hill's equation of muscle performance and its hidden insight on molecular mechanisms. *J. Gen. Physiol.* **142**, 561-573.
Seow, C. Y. and Fredberg, J. J. (2011). Emergence of airway smooth muscle functions related to structural malleability. *J. Appl. Physiol.* **110**, 1130-1135.
Silveira, P. S. P., Butler, J. P. and Fredberg, J. J. (2005). Length adaptation of airway smooth muscle: a stochastic model of cytoskeletal dynamics. *J. Appl. Physiol.* **99**, 2087-2098.
Silver, P. J. and Stull, J. T. (1984). Phosphorylation of myosin light chain and phosphorylase in tracheal smooth muscle in response to KCl and carbachol. *Mol. Pharmacol.* **25**, 267-274.
Smith, L. and Stull, J. T. (2000). Myosin light chain kinase binding to actin filaments. *FEBS Lett.* **480**, 298-300.
Smolensky, A. V., Ragozzino, J., Gilbert, S. H., Seow, C. Y. and Ford, L. E. (2005). Length-dependent filament formation assessed from birefringence increases during activation of porcine tracheal muscle. *J. Physiol.* **563**, 517-527.
Sobieszek, A. (1977). Ca-linked phosphorylation of a light chain of vertebrate smooth-muscle myosin. *Eur. J. Biochem.* **73**, 477-483.
Sobieszek, A. (2001). Vectorial phosphorylation of filamentous smooth muscle myosin by calmodulin and myosin light chain kinase complex. *J. Muscle Res. Cell Motil.* **22**, 505-511.
Surks, H. K., Richards, C. T. and Mendelsohn, M. E. (2003). Myosin phosphatase-Rho interacting protein. A new member of the myosin phosphatase complex that directly binds RhoA. *J. Biol. Chem.* **278**, 51484-51493.
Surks, H. K., Riddick, N. and Ohtani, K. (2005). M-RIP targets myosin phosphatase to stress fibers to regulate myosin light chain phosphorylation in vascular smooth muscle cells. *J. Biol. Chem.* **280**, 42543-42551.
Szeto, B. and Hai, C.-M. (1996). Length-dependent modulation of myosin phosphorylation and contractile force in coronary arterial smooth muscle. *Arch. Biochem. Biophys.* **329**, 241-248.
Taggart, M. J., Menice, C. B., Morgan, K. G. and Wray, S. (1997). Effect of metabolic inhibition on intracellular Ca^{2+}, phosphorylation of myosin regulatory light chain and force in rat smooth muscle. *J. Physiol.* **499**, 485-496.
Tang, D. D. and Gunst, S. J. (2001). Selected contribution: roles of focal adhesion kinase and paxillin in the mechanosensitive regulation of myosin phosphorylation in smooth muscle. *J. Appl. Physiol.* **91**, 1452-1459.
Tang, D. D., Wu, M.-F., Opazo Saez, A. MO. and Gunst, S. J. (2002). The focal adhesion protein paxillin regulates contraction in canine tracheal smooth muscle. *J. Physiol.* **542**, 501-513.
Trybus, K. M. (2000). Biochemical studies of myosin. *Methods* **22**, 327-335.
Uvelius, B. (1976). Isometric and isotonic length-tension relations and variations in cell length in longitudinal smooth muscle from rabbit urinary bladder. *Acta Physiol. Scand.* **97**, 1-12.
Wang, L., Paré, P. D. and Seow, C. Y. (2001). Selected contribution: effect of chronic passive length change on airway smooth muscle length-tension relationship. *J. Appl. Physiol.* **90**, 734-740.
Warshaw, D. M., Desrosiers, J. M., Work, S. S. and Trybus, K. M. (1990). Smooth muscle myosin cross-bridge interactions modulate actin filament sliding velocity in vitro. *J. Cell Biol.* **111**, 453-463.
Washabau, R. J., Wang, M. B., Dorst, C. L. and Ryan, J. P. (1991). Effect of muscle length on isometric stress and myosin light chain phosphorylation in gallbladder smooth muscle. *Am. J. Physiol.* **260**, G920-G924.
Washabau, R. J., Wang, M. B., Dorst, C. and Ryan, J. P. (1994). Role of myosin light-chain phosphorylation in guinea pig gallbladder smooth muscle contraction. *Am. J. Physiol.* **266**, G469-G474.
Wilson, D. P., Sutherland, C. and Walsh, M. P. (2002). Ca^{2+} activation of smooth muscle contraction: evidence for the involvement of calmodulin that is bound to the triton-insoluble fraction even in the absence of Ca^{2+}. *J. Biol. Chem.* **277**, 2186-2192.
Wingard, C. J., Browne, A. K. and Murphy, R. A. (1995). Dependence of force on length at constant cross-bridge phosphorylation in the swine carotid media. *J. Physiol.* **488**, 729-739.
Yamin, R. and Morgan, K. G. (2012). Deciphering actin cytoskeletal function in the contractile vascular smooth muscle cell. *J. Physiol.* **590**, 4145-4154.
Zhang, W. and Gunst, S. J. (2006). Dynamic association between alpha-actinin and beta-integrin regulates contraction of canine tracheal smooth muscle. *J. Physiol.* **572**, 659-676.
Zhang, W. and Gunst, S. J. (2017). Nonmuscle (NM) myosin heavy chain phosphorylation regulates the formation of NM myosin filaments, adhesome assembly and smooth muscle contraction. *J. Physiol.* doi: 10.1113/JP273906 [Epub ahead of print].